Similarity Solutions for Unsteady Hydromagnetic Free Convection Boundary Layer Flow over Flat Plates with Thermophoresis

M. Y. Ali[1,*], M. J. Uddin[1,2], M. N. Uddin[1], N. M. R. Zahed[1]

[1]Department of Mathematics, Chittagong University of Engineering & Technology, Chittagong-4349, Bangladesh

[2]Department of Electrical & Electronic Engineering, International Islamic University Chittagong, Chittagong-4318, Bangladesh

Abstract

This paper is focused on the analysis of thermophoresis on an unsteady two dimensional free convective boundary layer flow along a permeable inclined flat plate in the presence of magnetic field and thermophoresis. Governing time dependent partial differential equations are non- dimensionalzed and transformed into a system of nonlinear ordinary differential equations by applying similarity transformations. These are solved numerically by using the shooting method along with Runge-Kutta sixth order integration scheme. Numerical results for the dimensionless velocity, temperature and concentration profiles have been obtained and displayed graphically. The skin-friction coefficient, wall heat transfer coefficient and wall deposition flux rate have also been obtained and are presented in tabular form. The obtained numerical results also show that increased unsteadiness parameter significantly controls the thermophoretic particle.

Keywords: Boundary layer; Free convection; Hydro magnetic field; Similarity solution; Unsteady; Thermophoresis.

1. Introduction

Analysis of an unsteady hydro magnetic boundary layer flow and heat transfer of electrically conducting fluids is of great interest in many branches of engineering of the 21st century. Magneto hydrodynamics (MHD) is the study of the flow of electrically conducting fluids in a magnetic field. Many experimental and theoretical studies on conventional electrically conducting fluids indicate that magnetic field markedly changes their transport and heat transfer characteristics.

---
*
  Correspondingauthor: ali69cuet@gmail.com

Thermophores is with temperature dependent viscosity is an important mechanism of micro-particle transport due to a temperature gradient in the surrounding medium and has found numerous applications, especially in the field of aerosol. It is a phenomenon which causes small particles to be driven away from a hot surface and towards a cold one. The effects of thermal radiation on free convection flows are also important in the context of space technology and processes involving high temperatures. Goren [1] was one of the first to study the role of thermophoresis in laminar flow of a viscous and incompressible fluid. He used the classical problem of flow over a flat plate to calculate deposition rates and showed that substantial changes in surface depositions can be obtained by increasing the difference between the surface and free stream temperatures. This was later followed by similarity solutions of two dimensional laminar boundary layers and stagnation point flows by Gokoglu and Rosner [2], Park and Rosner [3]. Yeakub *et al.* [4] investigated the similarity solution of unsteady free convective laminar boundary flow around a vertical heated curvilinear surface. The combined effect of increasing the Prandtl number and the Grashof number reduces the thermal boundary layer thickness along the plates whichis vital in engineering application. Gupta [5] studied laminar free convection flow of an electrically conducting fluid past a vertical plate with uniform surface heat flux and variable wall temperature in presence of a magnetic field.

Many studies were reported considering the effect of thermophoresis on the boundary layer [6–8].The effects of thermophoresis and radiation on laminar flow werestudiedby Bakier and Gorla [9]. A paper by Postelnicu [10] dealt with the effects of thermophoreticparticledepositionon the natural convection flow over an inclined porous media. Goldsmith *et al.* [11] first studied the thermophoretic transport involved in a simple one-dimensional flow for the measurement of the thermophoreticvelocity. Wang [12] studied the combinedeffects of inertia, diffusion and thermophoresis on particledepositionfrom a stagnation point flow onto an axi-symmetricwavy wafer. Shen [13] analyzed the problem of thermophoreticdeposition of smallparticles on to cold surfaces in two-dimensional and axi-symmetric cases. Epstein *et al.* [14] analyzed the thermophoretic deposition of particles from a vertical plate in free convection boundary layer flow. Selim *et al.* [15] studied the effect of surface mass flux on mixed convective flow past a heated vertical flat permeable plate with thermophoresis. The similarity solutions to the convective heat transfer problems have been studied by Aziz [16] and Magyari [17] for an impermeable plate. Pop and Na [18] solved the boundary layer flow over a permeable stretching sheet in the presence of a magneticfield. Williams *et al.* [19] studied the unsteady free convection flow over a vertical flat plate under the assumption of variations of the wall temperature with time and distance. They found possible semi-similar solutions for a verity of classes of wall temperature distributions. Kumari *et al.* [20] observed that the unsteadiness in the flow fieldwascausedby the timedependentvelocity of the moving sheet. Ali and Magyari [21] presented the problem of unsteady fluid and heat flow induced by a submerged continuous surface while its steady motion is slowed down gradually. Alam *et al*. [22]

studied Dufour and Soret effect with variable suction on unsteady MHD free convection flow along a porous plate. Ali *et al.* [23] studied a case of similarity solution for unsteady laminar boundary layer flow in curvilinear surface. Mbeledogu and Ogulu [24] studied heat and mass transfer on unsteady MHD natural convection flow of a rotating fluid past a vertical porous flat plate in the presence of radiative heattransfer. Many authors have already studied the flow of dustyviscousfluidsuch as Kuiry and Bahadur [25] studied MHD flow of viscous fluid between two parallel porous plates with heat transfer in an inclined magnetic field and some of the important studies in the domain of dusty viscous fluid with elastic properties have been carried out by many researchers. Alam *et al.* [26] has analyzed the steady MHD boundary layer free convective heat and mass transfer flow over an inclined porous plate with variable suction and Soreteffect in presence of hall current. Madhura and Kalpana [27] have studied the thermal effect on unsteady flow of a dusty visco-elastic fluid between two parallel plates under different pressure gradients. Seth and Ansari [28] investigated the hydromagneticnatural convection flow past an impulsively moving vertical plate with ramped temperature in the presence of thermal diffusion and heat absorption.

Theoretical/experimental investigations of convective boundary layer flow with heat and mass transfer induced due to a moving surface with a uniform or non-uniform velocity play an important role in several manufacturing processes in industry which include the boundary layer flow along material handling conveyers, extrusion of plastic sheets, cooling of an infinite metallic plate in cooling bath, glass blowing, continuous casting and levitation, design of chemical processing equipment, formation and dispersion of fog, distribution of temperature and moisture over agricultural fields and groves of trees, damage of crops due to freezing, common industrial sight especially in power plants, etc. Seth *et al.* [29] discussed the hydromagneticnatural convection flow with heat and mass transfer of a chemically reacting and heat absorbing fluid past an accelerated moving vertical plate with ramped temperature and ramped surface concentration through a porous medium. An unsteady hydromagnetic natural convection flow past an infinite moving plate in a rotating medium has been studied by Seth *et al.* [30]. Seth and Sarker [31] considered the hydro magnetic natural convection flow with induced magnetic field and n^{th} order chemical reaction of a heat absorbing fluid past an impulsively moving vertical plate with ramped temperature. Seth *et al.* [32] has investigated effects of Hall current and rotation on hydromagnetic natural convection flow with heat and mass transfer of a heat absorbing fluid past an impulsively moving vertical plate with ramped temperature.

It is noticed that there may be an appreciable temperature difference between the surface of the solid body and ambient fluid in so many fluid flow problems of practical interests. This prompted many researchers to consider temperature dependent heat sources and/or sinks, which may have strong influence on heat transfer characteristics [33]. The researchers have studied heat generating and heat absorbing fluid flow is of considerable importance in several physical problems such as fluids undergoing

exothermic and endothermic chemical reaction, its applications in the field of nuclear energy [34].

The objective of this paper is to consider the effects of thermophoresis on unsteady, laminar, hydromagneticfree convection boundary layer two-dimensional flow along a semi-infinite, permeable inclined flat plates. A comprehensive parametric study is conducted and a representative set of graphical results for the velocity, temperature and concentration profiles are reported and discussed.

2.   **Mathematical Model**

In this work we considered the unsteady, laminar, hydromagnetic combined heat and mass transfer by natural convection flow along a continuously moving semi-infinite permeable flat plate that is inclined with an angle z from the vertical. With x-axis measured along the plate, a uniform magnetic field B_0 is applied in the y direction whichis normal to the flow direction. A heat source is placed within the flow to allow for possible heat generation effects. The fluid is assumed to be Newtonian, electrically conducting and heat generating. The governing continuity, momentum, energy and diffusion equations can be written as:

$$\frac{\partial u}{\partial x}+\frac{\partial v}{\partial y}=0 \tag{1}$$

$$\frac{\partial u}{\partial t}+u\frac{\partial u}{\partial x}+v\frac{\partial u}{\partial y}=\nu\frac{\partial^2 u}{\partial y^2}+g\beta(T-T_\infty)\cos z-\frac{\sigma B_0^2}{\rho}u \tag{2}$$

$$\frac{\partial T}{\partial t}+u\frac{\partial T}{\partial x}+v\frac{\partial T}{\partial y}=\frac{\lambda_g}{\rho c_p}\frac{\partial^2 T}{\partial y^2}+\frac{Q_0}{\rho c_p}(T-T_\infty) \tag{3}$$

$$\frac{\partial C}{\partial t}+u\frac{\partial C}{\partial x}+v\frac{\partial C}{\partial y}=D\frac{\partial^2 C}{\partial y^2}-\frac{\partial}{\partial y}(V_T C) \tag{4}$$

Where $u,$ $v$are the velocity components in the x and $y$directions respectively, $v$is the kinematic viscosity, g is the acceleration due to gravity, ρ is the density of the fluid, $\beta$is the volumetric coefficient of thermal expansion. T, T_w and T_∞ are the temperature of the fluid inside the thermal boundary layer, the plate temperature and the fluid temperature in the free stream, respectively, while C, C_w and C_∞ are the corresponding concentrations, σ is the electrical conductivity, B_0 is the uniform magnetic field, λ_g is the thermal conductivity of fluid, C_p is the specific heat at constant pressure, Q_0 is the heat generation coefficient, D is the molecular diffusivity of the species concentration and $V_T$is the thermophoretic velocity. The thermophoretic velocity$V_T$can be written as: $V_T=-K\upsilon\frac{\nabla T}{T_{ref}}=-\frac{K\upsilon}{T_{ref}}\frac{\partial T}{\partial y},$

Where k is the thermophoretic coefficient and T_{ref} is the referencetemperature.
The appropriate boundary conditions for the above model are as follows:

$$u = \frac{x}{t}, \; v = 0, \; T = T_w, \; C = 0 \quad at \; y = 0 \tag{5}$$

and $u = 0, \; T = T_\infty, \; C = C_\infty \qquad as \; y \to \infty$ (6)

The continuity equation (1) is satisfied by introducing the stream function $\psi(x, y)$
Such that $u = \dfrac{\partial \psi}{\partial y}, \; v = -\dfrac{\partial \psi}{\partial x}$

The momentum, energy and diffusion equations (2), (3) and (4) can be transformed to the corresponding ordinary differential equations by introducing the following similarity transformations:

$$x = \xi, \; t = \tau, \; \eta = y\sqrt{\frac{1}{2\nu t}}, \; \psi = x\sqrt{\frac{2\nu}{t}} f(\eta), \; \theta(\eta) = \frac{(T - T_\infty)}{(T_w - T_\infty)}, \; \phi(\eta) = \frac{C}{C_\infty}, \; u = \frac{x}{t} f' \tag{7}$$

The momentum, energy and diffusion equations (2) – (4) after some simplifications, reduce to the following forms:

$$f''' + (\eta + 2f)f'' - 2f'^2 + (2 - M)f' + Gr\theta \cos z = 0 \tag{8}$$

$$\theta'' + \Pr(2f + \eta)\theta' + \Pr Q\theta = 0 \tag{9}$$

$$\phi'' + Sc(\eta + 2f)\phi' - Sc(\phi\theta'' + \phi'\theta')Ta = 0 \tag{10}$$

Where,   Gr (Modified local Grashof number) $= \dfrac{2g\beta\tau^2 (T_w - T\infty)}{\xi}$,

Pr *(Modified* Pr *andtl number)* $= \dfrac{\gamma\rho c_p}{\lambda_g}$,   *M (Modified local Magnetic field Parameter)* $= \dfrac{\sigma B_0^2 2\tau}{\rho}$,

Q (Modified local heat generation Parameter) $= \dfrac{Q_0 2\tau}{\rho c_p}$,   *Sc (Schmidt number)* $= \dfrac{\nu}{D}$

Ta (Thermophoretic Parameter) $= -\dfrac{k(T_w - T_\infty)}{T_{ref}}$,

The corresponding boundary conditions are:

$$f = 0, \; f' = 1, \; \theta = 1, \; \phi = 0 \qquad as \; \eta = 0 \tag{11}$$

and $\qquad f' = 0, \; \theta = 0, \; \phi = 1 \quad as \; \eta \to \infty$ (12)

Where, the prime (′) denotes differentiation with respect to η.

The skin-friction coefficient, local Nusselt number (wall heat transfer coefficient), and local Stanton number (wall deposition flux):

The parameters of engineering interest for the present problem are the skin-friction coefficient, local Nusselt number and the local Stanton number which indicate physically wall shear stress, rate of heat transfer and wall deposition flux respectively. These can be obtained from the following expressions:
The skin-friction coefficient is given by

$$Cf_x(\text{Re}_x)^{\frac{1}{2}} = \frac{\tau_w}{\rho u^2} = f''(0), \quad \tau_w = \mu(\frac{\partial u}{\partial y})_{y=0}$$

The local Nusselt number may be written as

$$2Nu_x(\text{Re}_x)^{-\frac{1}{2}} = \frac{2xq_w}{(T_w - T_\infty)\lambda_g} = -\theta'(0), \quad q_w = -\lambda_g(\frac{\partial T}{\partial y})_{y=0}$$

and the Stanton number can be written as

$$St_x Sc(\text{Re}_x)^{\frac{1}{2}} = -\frac{J_s}{uC_\infty} = \phi'(0), \quad J_s = -D(\frac{\partial C}{\partial y})_{y=0}$$

Where, τ_w is the wall shear stress on the surface, q_w be the rate of heat transfer and J_s be the rate of transfer of species concentration.

3. Numerical Solution

The set of ordinary differential equations (8) to (10) with boundary conditions (11) and (12) are nonlinear and coupled. A standard initial value solver i.e., the shooting method is used to solve these equations numerically. For this purpose we applied the Nacthsheim-Swigert iteration technique [35]. In the process of iteration the velocity, temperature and concentration profile, the skin-friction coefficient, $f''(0)$, local Nusselt number (wall heat transfer coefficient), $\theta'(0)$ and local Stanton number (wall deposition flux), $\Phi'(0)$ are evaluated. The numerical results obtained for several selected values of the established parameters are displayed in graphs and tables below. These graphs and tables show that velocity, temperature, concentration, wall heat transfer coefficient, wall deposition flux and the skin-friction coefficient are affected significally with the variations of the considered controlling parameters.

4.   Results and Discussion

In order to assess the effects of the dimensionless thermo physical parameters on the regime calculations have been carried out on velocity field, temperature field, concentration field for various physical parameters like local heat generation parameter, Schmidt parameter, local magnetic field parameter and thermophoretic parameter. Due to free convection problem, positive value of $Gr = 6$ are taken which corresponds to a cooling problem and is generally encountered in nuclear engineering in connection with cooling of reactor. The parameters are chosen arbitrarily where $Pr = 0.71$ corresponds physically to air at 20°C, $Pr = 1.10$ corresponds to electrolyte

solution such as salt water and $Pr = 7.0$ corresponds to water, and $Sc = 0.30$ for helium and $Sc = 0.60$ water vapor at approximate 25°C and 1 atmosphere. We consider $60^0 = 60$ deg, $30^0 = 30$ deg, $20^0 = 20$ deg, $0^0 = 0$ deg in Figs. 4, 11 and 18. In order to get a physical insight into the problem, a representative set of numerical results are shown graphically in Figs. 1-21.

4.1. Velocity profiles

The values of Grashof number (Gr) are taken to be large from the physical point of view. The large Grashof number values correspond to free convection problem. The influence of the local Grashof number on the velocity is presented in Fig.1. The local Grashof number signifies the relative effect of the thermal buoyancy force to the viscous hydrodynamic force in the boundary layer. Fig. 1 represents the dimensionless velocity profiles along x- direction for several values of Gr. It is observed that the velocity profile decreases as the values of Grashof number increased, due to the increase of the buoyancy forces.
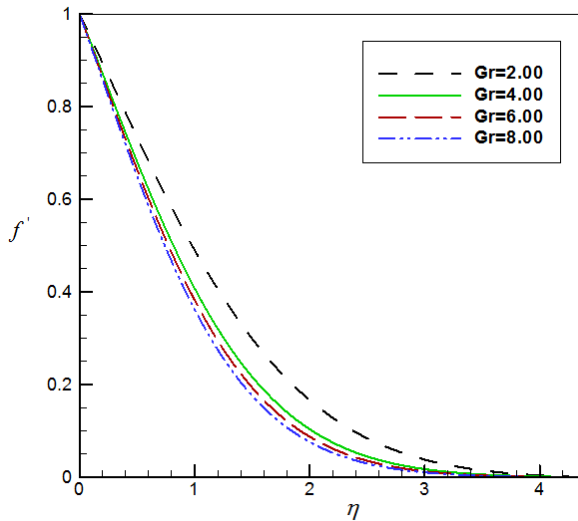
Fig. 1. Effect of dimensionless velocity profiles across the boundary layer for different values of Gr and for Pr = 0.71, M = 2.0, Q = 0.30, z = 30^0, Sc = 0.60, Ta = 1.50.

Fig. 2 illustrates the variation of dimensionless velocity profiles along x-direction for several value of prandtl number, Pr. From this figure we observe that the velocity profiles monotonically decreasing with the increase of prandtl number Pr.
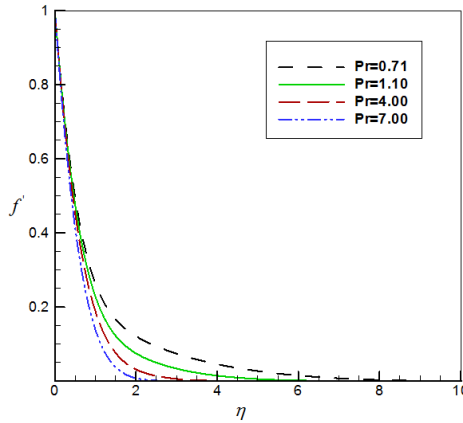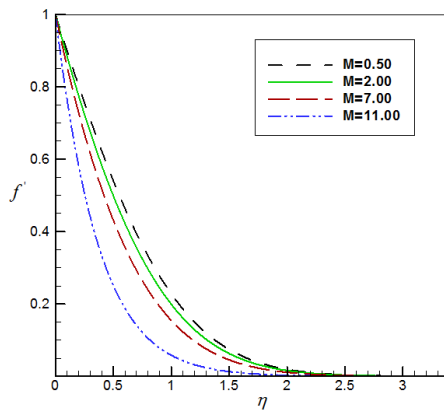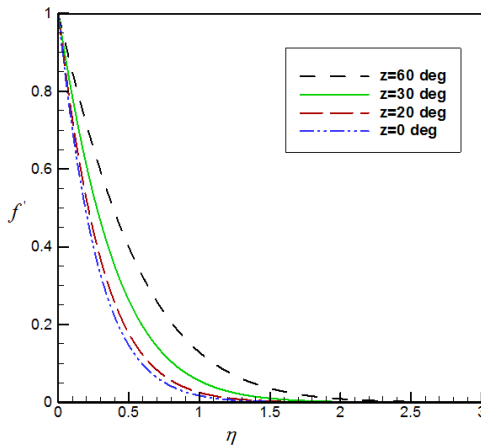
Fig. 2. Effect of dimensionless velocity profiles across the boundary layer for different values of Pr and for Gr = 6.0, M = 2.0, Q = 0.30, z = 30^0, Sc = 0.60, Ta = 1.50.

Fig. 3 displays the variation of dimensionless velocity profiles along *x*-direction for several value of local magnetic field parameter, *M*. The presence of a magnetic field normal to the flow in an electrically conducting fluid introduces a Lorentz force which acts against the flow. It is seen that the velocity profile decreases with increasing of the local magnetic field parameter, *M*.
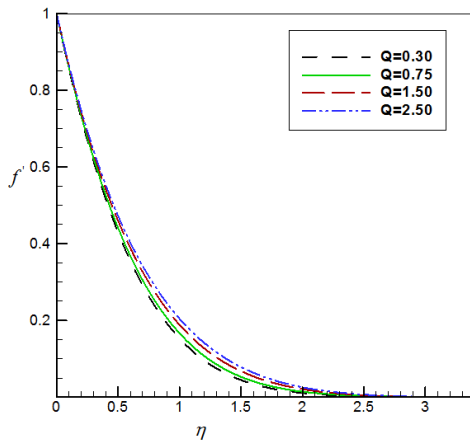

Fig. 3. Effect of dimensionless velocity profiles across the boundary layer for different values of M and for Gr = 6.0, Pr = 0.71, Q = 0.30, z = 30^0, Sc = 0.60, Ta = 1.50.

Representative velocity profiles for the typical angles of inclination $z = 60^0$, 30^0, 20^0, 0^0 are presented in Fig. 4. It is revealed from Fig. 4 that the velocity is decreased by decreasing the angle of inclination. The fact is that as the angle of inclination increases the effect of the buoyancy force due to thermal diffusion decreases by a factor of *z*.
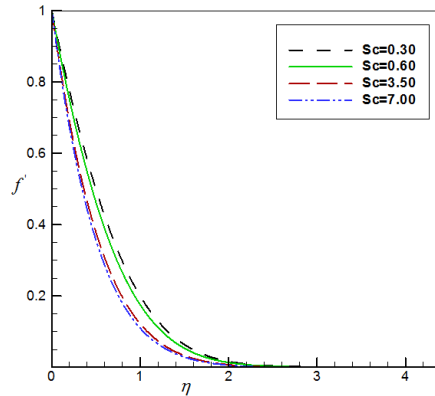
Fig. 4. Effect of dimensionless velocity profiles across the boundary layer for different values of z and for G r = 6.0, Pr = 0.71, M =2.0, Q = 0.30, Sc = 0.60, Ta = 1.50.

Fig. 5 exhibits the behavior of dimensionless velocity profiles along *x*-direction for some selected value of local heat generation parameter *Q*. From the Figure it is observed that when the heat is generated the buoyancy force increases, which induce the flow rate to increase giving, rise to the increase in the velocity profiles.

Fig. 5. Effect of dimensionless velocity profiles across the boundary layer for different values of Q and for Gr = 6.0, Pr = 0.71,M = 2.0, z = 30^0, Sc = 0.60, Ta = 1.50.

The effect of Schmidt number, *Sc* on the velocity profiles is shown in Fig. 6. It is clear that the fluid velocity decreases rapidly with the increase of Schmidt number.

Fig. 6. Effect of dimensionless velocity profiles across the boundary layer for different values of Sc and for Gr = 6.0, Pr = 0.71, M = 2.0, Q = 0.30, z = 30^0, Ta = 1.50.

Fig. 7 displays the variation of the dimensionless velocity profiles for some the values of the thermophoretic parameter *Ta*. The increase of the thermophoretic parameter *Ta* decreases the wall slope of the velocity profiles.
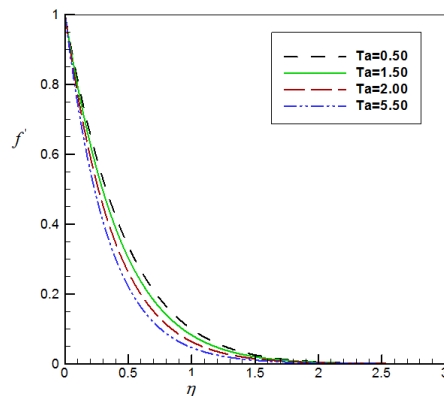

Fig. 7. Effect of dimensionless velocity profiles across the boundary layer for different values of T_a and for Gr = 6.0, Pr = 0.71, M = 2.0, Q = 0.30, z = 30^0, Sc = 0.60.

4.2. *Temperature profiles*

The dimensionless temperature profiles are presented in Figs. 8-14. The influence of the Grashof number on the temperature is presented in Fig. 8. As expected, it is observed that there is a rise in the velocity due to the enhancement of thermo buoyancy force. Here, the positive values of *Gr* correspond to cooling of the plate. This Figure displayed the variation of the dimensionless temperature profiles for some values of the Grashof number (*Gr*). We observe that the temperature profile increases monotonically as the value of Grashof number (*Gr*) increases.
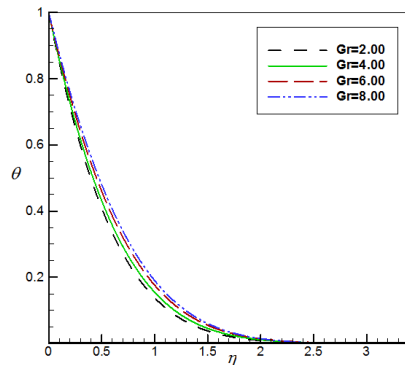
Fig. 8. Effect of dimensionless temperature profiles across the boundary layer for different values of Gr and for Pr = 0.71, M= 2.0, Q = 0.30, z = 30^0, Sc = 0.60, Ta=1.50.

The influence of Prandtl number (*Pr*) on temperature profiles is presented in the Fig. 9. It is observed that the temperature profile decreases with the increase of the Prandtl number *(Pr)*.
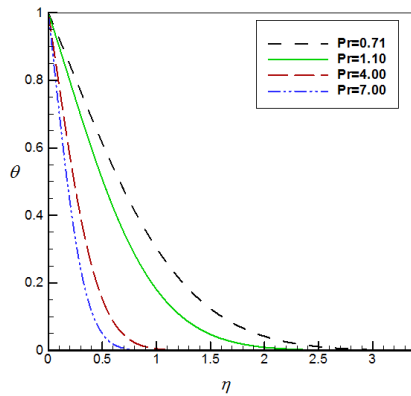

Fig. 9. Effect of dimensionless temperature profiles across the boundary layer for different values of Pr and for Gr = 6.0, M = 2.0, Q = 0.30, z = 30^0, Sc = 0.60, Ta = 1.50.

The dimensionless temperature profiles along x-direction for different values of local magnetic field parameter, *M* is presented in the Fig. 10. It is observed that the temperature profiles increase with the increase of the magnetic field parameter, which implies that the applied magnetic field tends to heat the fluid, and thus reduces the heat transfer from the wall.
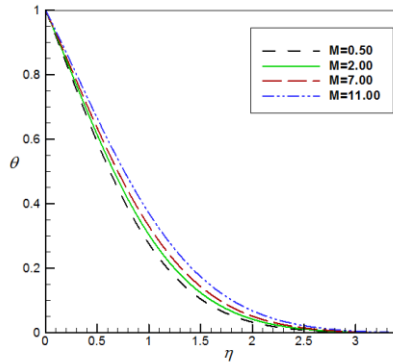
Fig. 10. Effect of dimensionless temperature profiles across the boundary layer for different values of M and for Gr = 6.0, Pr = 0.71, Q = 0.30, z = 30^0, Sc = 0.60, Ta = 1.50.

Fig. 11 shows the temperature profile for the variation of the angle of inclination *z*. It is clear that the temperature profile is slightly increased by decreasing the angle of inclination. We observe that the thermal boundary layer thickness increase as the angle of inclination increases.
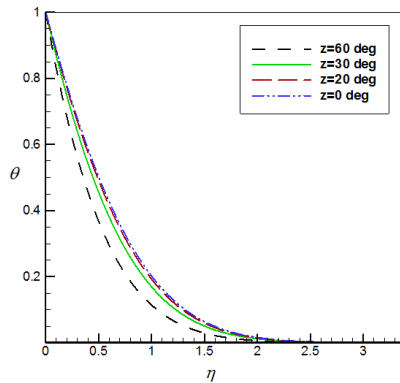

Fig. 11. Effect of dimensionless temperature profiles across the boundary layer for different values of z and for Gr = 6.0, Pr = 0.71, M = 2.0, Q = 0.30, Sc = 0.60, Ta = 1.50.

In Fig. 12 we have plotted the variation of the dimensionless temperature distribution for different values of *Q* and also showing the effects of the local heat generation parameter *Q*. The positive value of *Q* represents source i.e., heat generation in the fluid. For heat generation, the peak velocity occurs near the surface of the stretching plate. It can be seen that the temperature profiles rapidly increase when local heat generation parameter, *Q* increases which implies that owing to the presence of a heat source, the thermal state of the fluid increases causing the thermal boundary layer to increase.
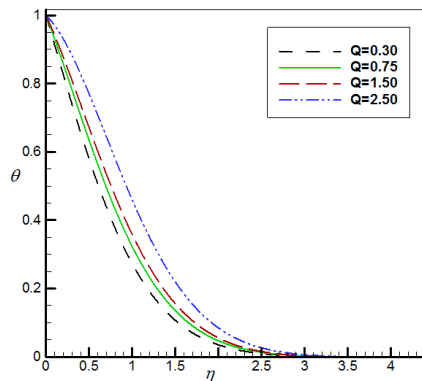
Fig. 12. Effect of dimensionless temperature profiles across the boundary layer for different values of Q and for G r= 6.0, Pr = 0.71, M = 2.0, z = 30^0, Sc = 0.60, Ta = 1.50.

The influence of various values of the Schmidt number, *Sc* is displayed in Fig. 13. From this figure we observe that the temperature profiles decrease swiftly with the increase of the Schmidt number, *Sc*.
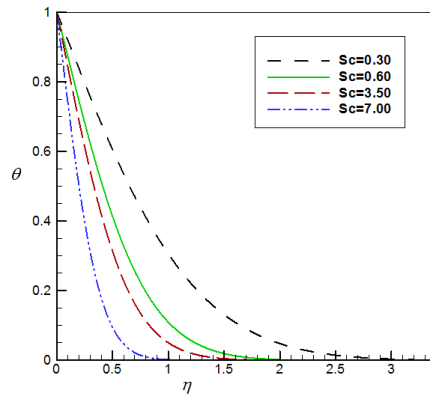

Fig. 13. Effect of dimensionless temperature profiles across the boundary layer for different values of Sc and for Gr = 6.0, Pr = 0.71, M = 2.0, Q = 0.30, z = 30^0, Ta = 1.50.

The effect of various values thermophoretic parameter *Ta*, on the temperature profiles is shown in Fig. 14. From this figure we find that the temperature profiles decrease rapidly with the increase of the thermophoretic parameter, *Ta*
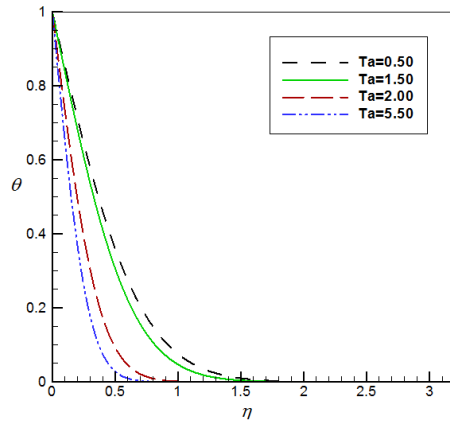
Fig. 14. Effect of dimensionless temperature profiles across the boundary layer for different values of Ta and for Gr = 6.0, Pr = 0.71, M = 2.0, Q = 0.30, z = 30^0, Sc = 0.60.

4.3. *Concentration profiles*

The dimensionless concentration profiles for the influence of various physical parameters are presented in Figs. 15-21.

Fig. 15 represents the effects of variation of the Grashof number (*Gr*) on the concentration profiles profile. From this Figure we see that the concentration profiles slightly increases with the increasing values of Grashof number (*Gr).*
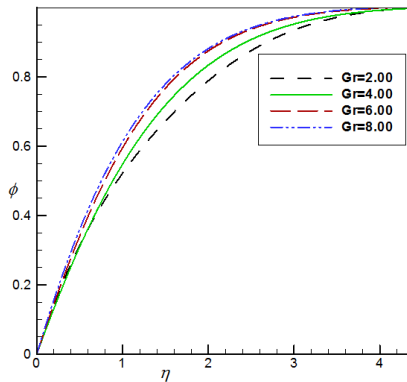

Fig. 15. Effect of dimensionless concentration profiles across the boundary layer for different values of *Gr* and for *Pr* = 0.71, *M* = 2.0, *Q* = 0.30, *z* = 30^0, *Sc* = 0.60, *Ta* = 1.50.

Fig. 16 displays the effects of the Prandtl number (*Pr*) on concentration profiles.It is noticed that the concentration profiles monotonically increases with the increasing values of Prandtl number (*Pr*).
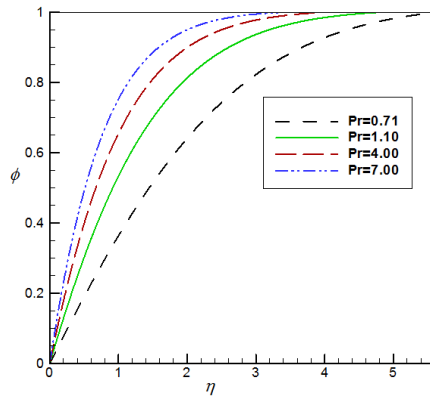
Fig. 16. Effect of dimensionless concentration profiles across the boundary layer for different values of Pr and for Gr = 6.0, M = 2.0, Q = 0.30, z = 30^0, Sc = 0.60, Ta = 1.50.

Illustrate the effect of the local magnetic field parameter is presented in the Fig. 17. The effect of an applied magnetic field is found to decrease the concentration profiles with the increasing of magnetic field parameter (*M*).
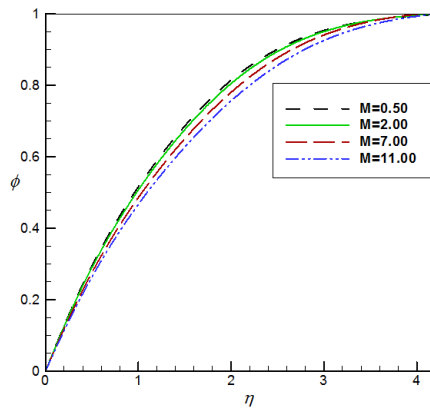

Fig. 17. Effect of dimensionless concentration profiles across the boundary layer for different values of M and for Gr = 6.0, Pr = 0.71, Q = 0.30, z = 30^0, Sc = 0.60, Ta = 1.50.

Fig. 18 exhibits the behavior of dimensionless concentration profiles along *x*-direction for the variation of the angle of inclination *z*. Here that concentration boundary layer thickness increase as the angle of inclination decreases.
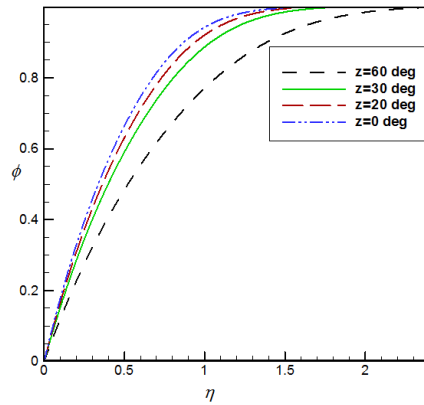
Fig. 18. Effect of dimensionless concentration profiles across the boundary layer for different values of z and for $Gr = 6.0$, $Pr = 0.71$, $M = 2.0$, $Q = 0.30$, $Sc = 0.60$, $Ta = 1.50$.

The dimensionless concentration profiles are displayed in Fig. 19 for various values of local heat generation parameter Q. That is in this figure we represent the dimensionless concentration profiles along x -direction for the various values of the effects of local heat generation parameter Q. As expected, the concentration profiles increase while the concentration boundary layer increases as the heat generation parameter (Q) increases.

Fig. 19. Effect of dimensionless concentration profiles across the boundary layer for different values of Q and for Gr = 6.0, Pr = 0.71, M = 2.0, z = 30^0, Sc = 0.60, Ta=1.50.

Fig. 20 reveals the effects of the Schmidt number, *Sc*. This is true only for small values of *Sc* for which the Brownian diffusion effect is large compared to the convection effect. However, for large values of *Sc* (*Sc* >1000) the diffusion effect is

minimal compared to the convection effect. It is also notified the fluid concentration increases rapidly with the increase of Schmidt number as we expected.
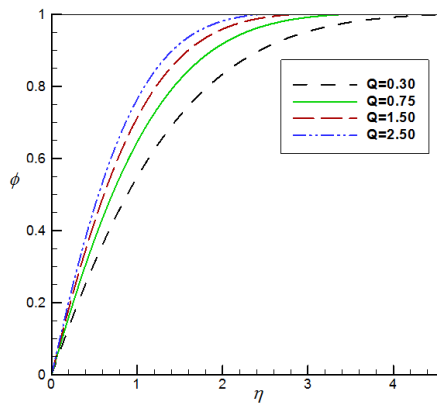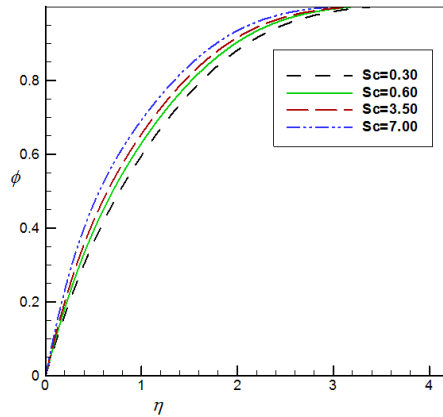

Fig. 20. Effect of dimensionless concentration profiles across the boundary layer for different values of Sc and for Gr = 6.0, Pr = 0.71, M = 2.0, Q = 0.30, z = 30^0, Ta = 1.50.

The effect of the thethermophoretic parameter (*Ta*) concentration fields is shown in Fig. 21. In this figure we can see that the concentration profiles swiftly decreases with the increase of the thermophoretic parameter (*Ta*).

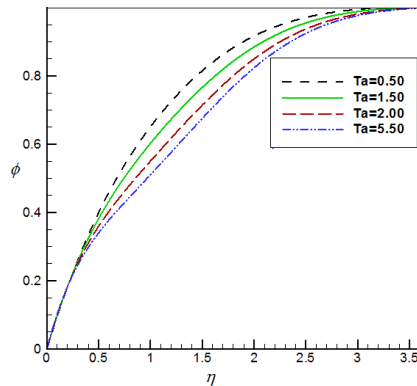Fig. 21. Effect of dimensionless concentration profiles across the boundary layer for different values of *Ta* and for *Gr* = 6.0, *Pr* = 0.71, *M* = 2.0, *Q* = 0.30, *z* = 30^0, *Sc* = 0.60.

The skin-friction coefficient, *f″*(0), local Nusselt number (wall heat transfer coefficient), *θ′*(0) and local Stanton number (wall deposition flux), *Φ′*(0) are important physical parameters. These tables are given below.

Table 1. Skin-friction coefficient, f''(0), local Nusselt number (wall heat transfer coefficient), θ′(0) and local Stanton number (wall deposition flux), Φ′(0) for different values of Gr.

Gr	f''(0)	θ′(0)	Φ′(0)
2.00	2.2598586	0.67685952	0.7648342
4.00	2.1956669	0.68442687	0.7693142
6.00	2.1321237	0.69174480	0.7736717
8.00	1.3464151	0.76199768	0.8174619

Table 2. Skin-friction coefficient, f''(0), local Nusselt number (wall heat transfer coefficient), θ′(0) and local Stanton number (wall deposition flux), *Φ*′(0) for different values of Pr.

Pr	f''(0)	θ′(0)	Φ′(0)
0.71	1.5193656	0.74251013	0.8053211
1.10	1.5343276	0.97037073	0.8027338
4.00	1.5696385	2.07686583	0.7976892
7.00	1.5805795	2.83711476	0.7963113

Table 3. Skin-friction coefficient, f''(0), local Nusselt number (wall heat transfercoefficient), θ′(0) and local Stanton number (wall deposition flux), Φ′(0) for different values of M.

M	f''(0)	θ′(0)	Φ′(0)
0.50	1.0099780	0.79340950	0.8373123
2.00	1.5193656	0.74251013	0.8053211
7.00	2.6693046	0.64660518	0.7471340
11.00	2.8943719	0.57452283	0.7253033

Table 4. Skin-friction coefficient, f''(0), local Nusselt number (wall heat transfer coefficient), θ′(0) and local Stanton number (wall deposition flux), Φ′(0) for different values of z.

z	f''(0)	θ′(0)	Φ′(0)
60^0	1.5622929	0.73744999	0.8021965
30^0	1.5193656	0.74251013	0.8053211
20^0	1.5113005	0.74344964	0.8059024
0^0	1.5044013	0.74425058	0.8063984

Table 5. Skin-friction coefficient, f''(0), local Nusselt number (wall heat transfer coefficient), θ′(0) and local Stanton number (wall deposition flux), Φ′(0) for different values of *Q*.

Q	f''(0)	θ′(0)	Φ′(0)
0.30	1.5236619	0.86502531	0.8073958
0.75	1.5193656	0.74251013	0.8053211
1.50	1.4980298	0.54648898	0.8048472
2.50	1.4235147	0.29711647	0.8014301

Table 6. Skin-friction coefficient, f''(0), local Nusselt number (wall heat transfer coefficient), θ′(0) and local Stanton number (wall deposition flux), Φ′(0) for different values of *Sc*.

Sc	f''(0)	θ′(0)	Φ′(0)
0.30	1.5200799	0.78195608	0.5980554
0.60	1.5211119	0.78424216	0.8931511
3.50	1.5212197	0.78520643	2.4728101
7.00	1.5212198	0.78620636	3.6780359

Table 7. Skin-friction coefficient, f"(0), local Nusselt number (wall heat transfer coefficient), θ′(0) and local Stanton number (wall deposition flux), Φ′(0) for different values of *Ta*.

Ta	f"(0)	θ′(0)	Φ′(0)
0.50	1.5212167	0.78421884	4.5954021
1.50	1.5211908	0.78432149	6.6295469
2.00	1.5211676	0.78441020	7.4910241
5.50	1.5208914	0.78477588	11.5117634

The numerical results are illustrated in Tables 1 to 7 for the effects of various parameters on the Skin-friction coefficient, local Nusselt number, local Stanton number. From Tables 1, 4 and 7 it is clear that the Skin-friction coefficient decreases while the local Nusselt number and local Stanton number increase with the increase of the Grashof number (*Gr*), decrease the angle of inclination (*z*) and increase the thermophoretic parameter (*Ta*) respectively. From Table 2 we observe that with the increase of Prandtl number (*Pr*), the Skin-friction coefficient increases while the local Nusselt number and the local Stanton number decrease. For the the increase of the local Magnetic field parameter (*M*), the Skin-friction coefficient and the local Nusselt number increase while the local Stanton number decreases as shown in Table 3. The Skin-friction coefficient and the local Stanton number decrease (Table 5) while the local Nusselt number increases with the increase of local heat generation parameter (*Q*). Table 6 revels that the Skin-friction coefficient and the local Stanton number increase while the local Nusselt number decreases with the increase of Schmidt number (*Sc*).

5. Conclusion

A mathematical model has been presented for the unsteady free convection boundary layer flow about flat plate in viscous incompressible fluid in presence of magnetic field with thermophoresis. In the present work, we make attempt to investigate the problem of an unsteady hydromagnetic free convection boundary layer flow over flat plates with thermophoresis. The results are analyzed for various physical parameters such as local magnetic field parameter, local Grashof number, Prandtl number, Schmidt number, local heat generation parameter, magnetic parameter, thermophoretic parameter, inclined plate, heat and mass transfer characteristics. Following conclusion can be drawn from the present investigations:

a. The influences of thermophoresis and variable liquid properties can act simultaneously and their interactions must be considered for the accurate prediction of heat and mass transfer rates and other effects.
b. The effect of thermophoresis is dominating on the velocity, temperature and concentration profiles. So using it boundary layer growth can be stabilized.
c. In free convection regime fluid velocity and concentration boundary layer increase whereas thermal boundary layer decreases with the increase of the local heat generation parameter.

d.   The increase of angle of inclination decreases the local Nusselt number and the local Stanton number.
e.   Thermophoretic particle deposition increases the rate of mass transfer on the wall.
f.   Using magnetic field we can control the heat and mass transfer flow characteristics.
g.   Thermophoretic parameter plays a considerable role on concentration profiles.

Finally, it is hoped that this mathematical model can be used as a vehicle for understanding the thermophoresis particle deposition on heat and mass transfer produced in unsteady free convection boundary-layer flow past an inclined flat plates in the presence of a magnetic field and heat generation. The results of the study are of great interest because flows over flat plates play a predominant role in applications of science and engineering, as well as in many transport processes in nature.

References

1.   S. L. Goren, J. Colloid Interface Sci. **61**, **77** (1977). http://dx.doi.org/10.1016/0021-9797(77)90416-7
2.   S. A. Gokoglu and D. E. Rosner, AIAA J. **24**, 172 (1986). http://dx.doi.org/10.2514/3.9239
3.   H. M. Park and D. E. Rosner, Chem. Eng. Sci. **44**, 2233 (1989). http://dx.doi.org/10.1016/0009-2509(89)85158-9
4.   M. Y.Ali and M. M. T. Hossain, Int. J. Appl. Math Stat. **30**, 1 (2012).
5.   A. S. Gupta, Z Angew Math. Phys. **13**, 3243 (1963).
6.   L. Talbot, R. K. Cheng, R. W. Schefer, and D. R. Willis, J. Fluid Mech. **101**, 737 (1980). http://dx.doi.org/10.1017/S0022112080001905
7.   G. K. Batchelor and C. Shen, J. Colloid Interface Sci. **107**, 21 (1985). http://dx.doi.org/10.1016/0021-9797(85)90145-6
8.   S. Jayaraj, K. K. Dinesh, and K. L. Pallai, Heat Mass Transfer **34**, 469 (1999). http://dx.doi.org/10.1007/s002310050284
9.   A. Y. Bakier and R. S. R. Gorla, Heat Mass Transfer **47(4)**, 419 (2011). http://dx.doi.org/10.1007/s00231-010-0702-7
10.   A. Postelnicu, Int. J. Heat Mass Transfer **55**, 2087 (2012). http://dx.doi.org/10.1016/j.ijheatmasstransfer.2011.12.011
11.   P. Goldsmith and F. G. May, Diffusiophoresis and Thermophoresis in Water Vapour Systems, in: C.N. Davies (Ed.), Aerosol Science (Academic Press, London, 1966) pp. 163–194.
12.   C. C. Wang, Int. J. Heat Mass Transfer **49**, 1395 (2006). http://dx.doi.org/10.1016/j.ijheatmasstransfer.2005.09.036
13.   C. Shen, J. Colloid Interface Sci. **127**, 104 (1989). http://dx.doi.org/10.1016/0021-9797(89)90011-8
14.   M. Epstein, G. M. Hauser, and R. E. Henry, J. Heat Transfer, **107**, 272 (1985). http://dx.doi.org/10.1115/1.3247410
15.   A. Selim, M. A. Hossain, and D. A. S. Rees, Int. J. Thermal Sci. **42**, 973 (2003). http://dx.doi.org/10.1016/S1290-0729(03)00075-9
16.   A. Aziz, Comm. Nonlinear Sci. Numer. Simulat. **14**, 1064 (2009). http://dx.doi.org/10.1016/j.cnsns.2008.05.003

17. E. Magyari, Int. J. Therm. Sci. **47**, 1436 (2008). http://dx.doi.org/10.1016/j.ijthermalsci.2007.12.010
18. I. Pop and T. Y. Na, Mech. Res. Commun. **25(3)**, 263 (1998). http://dx.doi.org/10.1016/S0093-6413(98)00037-8
19. J. C. Williams, J. C. Mulligan, and T. B. Rhyne, J. Fluid Mech. **175**, 309 (1987). http://dx.doi.org/10.1017/S0022112087000405
20. M. Kumari, A. Slaouti, S. Nakamura, H. S. Takhar, and G. Nath, ActaMechanica **116**, 75 (1986). http://dx.doi.org/10.1007/BF01171421
21. M. E. Ali and E. Magyari, Int. J. Heat Mass Transfer **50**, 188 (2007). http://dx.doi.org/10.1016/j.ijheatmasstransfer.2006.06.021
22. M. S. Alam, M. M. Rahman, and M. A. Samad, Nonlinear Analysis: Modeling and Control, **11**, 217 (2006).
23. M. Y. Ali, and M. G. Hafez, ARPN J. Eng. Appl. Sci. **7(6)**, 731 (2012).
24. I. U. Mbeledogu and A. Ogulu, Int. J. Heat Mass Transfer **50**, 1902 (2007). http://dx.doi.org/10.1016/j.ijheatmasstransfer.2006.10.016
25. D. R. Kuiry and S. Bahadur, J. Sci. Res. **7(3)**, 21 (2015). http://dx.doi.org/10.3329/jsr.v7i3.22574
26. M. S. Alam, M. Ali, M. A. Alim, and A. Saha, J. Sci. Ind. Res. **49**, 155 (2014). http://dx.doi.org/10.3329/bjsir.v49i3.22129
27. K. R. Madhura and G. Kalpana, Int. J. Engg. Technol. **2(2)**, 88 (2013). http://dx.doi.org/10.14741/ijcet/spl.2.2014.16
28. G. S. Seth and M. S. Ansari, Int. J. Appl. Mech. Eng. **15(1)**, 199 (2010).
29. G. S. Seth, S. M. Hussain, and S. Sarker, J. Egypt. Math. Soc. **23**, 197 (2015).
30. G. S. Seth, R. Nandkeolyar, and M. S. Ansari, Int. J. Appl. Math. Mech. **7(21)**, 52 (2011).
31. G. S. Seth and S. Sarker, Bulg. Chem. Commun. **47(1)**, 66 (2015).
32. G. S. Seth, R. Sharma, and S. Sarker, J. Appl. Fluid Mech. **8(1)**, 7 (2015).
33. K. Vajravelu and J. Nayfeh, Int. Commun. Heat Mass Transfer **19**, 701 (1992). http://dx.doi.org/10.1016/0735-1933(92)90052-J
34. J. C. Crepeau and R. Clarksean, ASME J. Heat Transfer **119**, 183 (1997). http://dx.doi.org/10.1115/1.2824086
35. S. T. Khaleque and M. A. Samad, Res. J. Appl. Sci. Eng. Technol. **2(4)**, 368 (2010).